REPORT DOCUMENTATION PAGE

Form Approved
OMB No. 0704-0188

1. REPORT DATE *(DD-MM-YYYY)*	2. REPORT TYPE	3. DATES COVERED *(From - To)*
	Technical Paper	

4. TITLE AND SUBTITLE

Please see attached

5a. CONTRACT NUMBER

5b. GRANT NUMBER

5c. PROGRAM ELEMENT NUMBER

6. AUTHOR(S)

5d. PROJECT NUMBER
2308

5e. TASK NUMBER
M13C

5f. WORK UNIT NUMBER
346057

7. PERFORMING ORGANIZATION NAME(S) AND ADDRESS(ES)

ERC

8. PERFORMING ORGANIZATION REPORT

9. SPONSORING / MONITORING AGENCY NAME(S) AND ADDRESS(ES)

Air Force Research Laboratory (AFMC)
AFRL/PRS
5 Pollux Drive
Edwards AFB CA 93524-7048

10. SPONSOR/MONITOR'S ACRONYM(S)

11. SPONSOR/MONITOR'S NUMBER(S)
Please see attached

12. DISTRIBUTION / AVAILABILITY STATEMENT

Approved for public release; distribution unlimited.

13. SUPPLEMENTARY NOTES

14. ABSTRACT

15. SUBJECT TERMS

16. SECURITY CLASSIFICATION OF:			17. LIMITATION OF ABSTRACT	18. NUMBER OF PAGES	19a. NAME OF RESPONSIBLE PERSON
a. REPORT	b. ABSTRACT	c. THIS PAGE			Leilani Richardson
Unclassified	Unclassified	Unclassified	A		19b. TELEPHONE NUMBER *(include area code)* (661) 275-5015

2307 A113C

MEMORANDUM FOR PRS (In-House Contractor Publication)

FROM: PROI (STINFO) 17 April 2002

SUBJECT: Authorization for Release of Technical Information, Control Number: **AFRL-PR-ED-TP-2002-084** Bruce Chehroudi (ERC); Doug Talley (PRSA), "The Fractal Geometry of Round Turbulent Cryogenic Nitrogen Jets at Subcritical and Supercritical Pressures"

Journal entitled "Atomization and Sprays" **(Statement A)**
(Deadline: 17 May 2002)

1. This request has been reviewed by the Foreign Disclosure Office for: a.) appropriateness of distribution statement, b.) military/national critical technology, c.) export controls or distribution restrictions, d.) appropriateness for release to a foreign nation, and e.) technical sensitivity and/or economic sensitivity.
Comments:_____

Signature _____ Date _____

2. This request has been reviewed by the Public Affairs Office for: a.) appropriateness for public release and/or b) possible higher headquarters review.
Comments: _____

Signature _____ Date _____

3. This request has been reviewed by the STINFO for: a.) changes if approved as amended, b) appropriateness of references, if applicable; and c.) format and completion of meeting clearance form if required
Comments:_____

Signature _____ Date _____

4. This request has been reviewed by PR for: a.) technical accuracy, b.) appropriateness for audience, c.) appropriateness of distribution statement, d.) technical sensitivity and economic sensitivity, e.) military/ national critical technology, and f.) data rights and patentability
Comments:_____

APPROVED/APPROVED AS AMENDED/DISAPPROVED

_____

PHILIP A. KESSEL Date
Technical Advisor
Space and Missile Propulsion Division

The Fractal Geometry of Round Turbulent Cryogenic Nitrogen Jets at Subcritical and Supercritical Pressures

B. Chehroudi[*] *and* *D. Talley*[+]

[*] *Engineering research Corporation*
Principal Scientist
(Corresponding Author)

+Air Force Research Laboratory
AFRL/PRSA Propulsion Directorate
Edwards AFB, CA 93524-7680

Submitted to

Atomization & Sprays

Dept. Mechanical Engineering
Carnegie Mellon University
Pittsburgh, PA 15213-3890

(March, 2002)

Abstract

Box-counting and EDM methods were used to measure the fractal dimension of round turbulent cryogenic nitrogen jets at pressures ranging from subcritical to supercritical pressures. Both method produced similar trends, with close quantitative agreement for a suitably small box-counting scale. At subcritical pressures, the fractal dimension was found to be consistent with the fractal dimension of a spray in the 2nd wind-induced atomization regime. The fractal dimension tended to increase as pressure increased, until at supercritical pressures the fractal dimension was found to be consistent with that of gas jets and mixing layers. The results constitute additional quantitative evidence for the hypothesis that subcritical jets exhibit mainly spray-like behavior, while supercritical jets exhibit mainly gas-like behavior. This appears to have been the first time pressure effects on the fractal dimension of turbulent jets has been measured.

Introduction

As combustion chamber pressures become increasingly higher in order to realize performance and/or efficiency benefits in a wide range of propulsion and energy conversion applications, the injected fluid(s) may experience ambient pressures exceeding the critical pressure(s) of the propellants. For example, in the cryogenic liquid hydrogen/liquid oxygen Space Shuttle Main Engine, the thrust chamber pressure is about 22.3 MPa, and thrust chamber pressures for the oxygen/hydrogen Vulcain engine used to launch the Ariane 5 vehicle have been recorded to reach up to 10 MPa. Both of these pressures exceed the critical pressure of 5.043 MPa for liquid oxygen. In many applications, including liquid rockets, the initial temperature of the propellant is often below the critical temperature, and later heats up to a supercritical temperature as it is mixed and burned in the combustion chamber.

As chamber pressures approach and exceed the critical pressure, combustion mechanisms can be expected to become distinctly different than conventional spray combustion processes at low pressures. For example, for single component fluids, the distinct difference between the gas and liquid phases disappears when the pressure exceeds the critical pressure or the temperature exceeds the critical temperature. Surface tension and the enthalpy of vaporization vanish, and large variations in the density, thermal conductivity, and mass diffusivity occur near the critical point. For multicomponent fluids, the solubility of the gas phase in the liquid phase increases as pressure approaches the critical pressure, and mixture effects need to be taken into account in calculating the critical properties. When mixture effects are considered, the critical pressure of a mixture can be found to be several times the critical pressure of the propellant of interest. Understanding and modeling the effect of these differences on the shear layer of the injected propellant are vital to understanding the mixing and performance characteristics of these high performance engines.

Until recently, understanding of the injection process under these conditions has been limited. However, recent experimental and theoretical work, motivated to a large extent by liquid rocket combustion applications, has begun to allow a picture of the shear layer dynamics to emerge. See for example, *Mayer et al. [1,2], Chen and Sui [3], Woodward and Talley [4], Harstad and Bellan [5], Delplanque and Sirignano [6], Oefelein and Yang [7]*, and *Chehroudi et al. [8, 9]*. One of the important experimental findings was the transition in the morphology of the injected jet boundary as chamber pressure increases from a subcritical to supercritical pressure. *Chehroudi et al. [8,9]* studied cryogenic liquid nitrogen jets (simulating liquid oxygen in liquid rocket engines) injected into room temperature nitrogen at various subcritical and supercritical pressures. The initial

temperature of the jet was between 90 and 110 K, which is below the critical temperature of 126.2 K for nitrogen. Back-illuminated visualizations of the results are shown in Fig. 1. It was found that at subcritical chamber pressures, the jet appears to be liquid-like with instabilities that grow downstream of the injector. In the shear region, very fine drops are found to be ejected from the jet. Major structural changes occur as the pressure is increased to near the critical pressure. Drops are no longer detected in the shear region. These drops are replaced by small comb-like ligaments which "dissolve" into the surrounding media due to the combined effects of the reduction in surface tension and negligible latent heat of vaporization. As chamber pressure is increased further beyond the critical pressure, the jet begins to take on the appearance of a turbulent gas jet injected into a gaseous environment. A quantitative examination of the shear layer growth rate, using both high-speed back-lit images and Raman scattering data, also indicates that the growth rate of the jet was consistent with that of round sprays at subcritical pressures, and consistent with that of shear layers surrounding gas jets at supercritical pressures. See *Chehroudi et al. [10]* for more details.

This metamorphic change of the cryogenic jet or shear layer boundary was the motivation for investigating the change in the fractal dimension of the boundary in the present study. The objective was to further quantify the extent to which the jets may behave like conventional sprays at subcritical pressures, but like gas jets at supercritical pressures. The present study appears to be the first time the fractal dimension of jets has been investigated over a range of subcritical to supercritical pressures.

The Fractal Dimension

The notion of a fractal has been given a strong foundation and application by its founder *Mandelbrot [11]*, and is intimately connected to the concept of scaling and self-similarity. *Peitgen, et. al. [12]* pointed out that in examining the structure of a cauliflower, the head may be found to be composed of several branches or parts, which when removed and compared with the whole are very much similar in shape to the whole, only smaller. The parts can in turn be decomposed into even smaller parts, which again are very much similar in shape to the whole as well as to the first generation of parts. This self-similarity as a function of scale only carries through for about three to four stages, after which the cauliflower is no longer self similar. The scales over which self similarity applies is said to range from an inner, or smallest, scale, to an outer, or largest, scale.

The concept of dimension in mathematics has a historical evolution. In Euclidean geometry, a line, a plane, and a surface in space have dimensions of one, two, and three respectively. In topology, things are slightly different. For example, a straight line and any non-self-intersecting curve are equivalent and have the same "topological dimension." Finally, these concepts were shaken by the introduction of the so-called "space-filling" curves. Given some patch of a plane, there exists a "space-filling" curve which meets every point in that patch. Thus, a curve, which by nature is something one-dimensional, can fill something two-dimensional. This questions the intuitive perception of curves as one-dimensional objects, because they fill the plane, an object which is intuitively perceived as two-dimensional. Looking at a self-similar curve with the notion defined in relation to the cauliflower, there is a power law relation between the number of pieces, N, and the reduction factor, ε, as: $N = (1/\varepsilon)^{D_s}$. In other words, this power-law relationship states that if a self-similar curve is reduced by, say, $\varepsilon = 1/2$, the number of similar pieces increases by 2^{D_S} . The quantity D_S is defined as the "self-similarity dimension" of the curve. Obviously, for a line, a square, and a cube, we have D_S=1, 2, 3, respectively, which happen to be the topological dimensions. For self-similar curves this dimension is determined through an exercise to measure the total length of the curve using rulers with

different compass settings (or yardstick lengths). The reciprocal compass setting can be considered to be the precision of the length measurement. Mechanistically, one selects a fixed compass setting and attempts to find the number of compass settings needed to cover the entire curve. In other words, one measures the total length of the curve using a fixed setting of the compass. This is repeated for different compass settings. Plotting the number of compass lengths required to cover the curve at a given compass setting as a function of the reciprocal compass setting itself traces a line in a log-log plot for a self-similar curve. The slope of this line, d, and the self-similarity dimension, D_S, can be shown related by: $D_S = 1 + d$, where d is positive in magnitude. Usually, however, the number of compass lengths at a given fixed setting is plotted against the compass setting itself (which in this case, $D_S = 1 - d$ as d is negative in magnitude). Motivated by this result for self-similar curves, the fractal (compass) dimension for shapes that are not strictly self-similar curves such as the jet boundary we would like to analyze are defined as: $D_C = 1 + d$. With this, the fractal dimension of the coast of the England that has many wrinkles is 1.36 whereas the that of the state border of Utah having smooth straight lines is equal to 1. Note that a non-integer number is attributed to the dimension (fractal). The fractal dimension of any curve is between 1 and 2 and the more wrinkled and "space-filling" it looks the larger the dimension value becomes. Natural curves, similar to a cauliflower, are self-similar only to within a narrow range of scales. Our objective here is to measure the fractal dimension of the interface of the jets injected into the chamber to examine if any pattern is uncovered. To our knowledge, this is the first application of the fractal approach to the liquid jet interface under high pressures up to supercritical conditions.

Practical Measurement of the Fractal Dimension

In the literature there are several methods to determine the fractal dimension of a boundary. For example the above-mentioned ruler method is also called the caliper method or the arc-swinging method. This method is difficult to implement for computer analysis, so more computer-compatible and faster algorithms have been devised. One popular method for evaluating the fractal dimension is referred to as box-counting, or the Kolmogrov dimension (see *Russ [13], [14], and Kaye [15]*). One overlays the curve on a square grid with mesh size ε and counts the number of grid boxes which contain any part of the curve. This gives a number $N(\varepsilon)$ which depends on the mesh size ε. The negative of the slope of the line fitted to the linear section of the plot of $\log[N(\varepsilon)]$ *vs.* $\log(\varepsilon)$ is the box-counting dimension. Another approach leads to what is referred to as Minkowski dimension, see *Russ [13]*. In this method, the center of a circle with radius ε is swept continuously along the curve. This creates what is known as a Minkowski sausage around the curve. The area of the sausage as a function of the radius of the circle is drawn on a log-log plot. The Minkowski dimension is equal to (2 – the slope of the linear region). In this paper both box-counting and Minkowski methods are used to calculate the fractal dimension. For the latter method, the Euclidean Distance Mapping (EDM) algorithm of *Russ [13]* is implemented. Consider a black object in a white background where the fractal dimension of the boundary between the two is desired. EDM is an image processing operation that is applied to a black and white image to produce a gray-scale image in which each black pixel is given a brightness value equal to its distance from the nearest white background point. Therefore, the larger the distance of a pixel from the nearest border the higher its assigned gray-scale intensity value, being linearly proportional to the distance. The same procedure can assign values to the white background pixels based on their distance from the nearest point on the object. Thresholding the distance map for either the object or the background produces uniform erosion and dilation of the boundary to any desired distance from the original boundary, without iteration. The EDM method is superior to the classical erosion/dilation method, see *Russ [14]*. It is really not necessary to perform the thresholding operations. Counting the pixels as a function of their brightness (distance) values produces a plot that directly

provides the Minkowski dimension. Both Box-counting and Minkowski methods are shown to provide reliable results, see *Hall et al [16]*. However, the EDM algorithm in determining the fractal dimension is more isotropic, more efficient, and generally more precise than the box-counting method, and easy to implement on a computer, see *Russ and Russ [17]*. Both techniques are limited to only self-similar and not self-affine boundaries.

Fractal Analysis of Cryogenic Jets

Before running the fractal analysis program for the computation of fractal dimensions, the images need to be conditioned. In particular, corrections to images are applied to account for the reference background condition. Then smoothing and twice-sharpening filters are applied. Also, an appropriate pixel intensity threshold level (described later) is selected to identify the boundary of the jet injected into the chamber. A 200X200 pixel image of a square boundary within our 432 x 477 full frame size is used as a test image to evaluate the fractal analysis program. Theoretically, the fractal dimension of the smooth boundary of this square must be equal to one. The analysis, however, gives a fractal dimension higher than one by at most 3% for the box-counting and EDM methods. For the box-counting dimension, two different methods are used to change the mesh size. In one case, the mesh size is increased by the following sequence, 1x1, 2x2, 3x3,..., 32x32 pixels, and in the other by 2x2, 4x4, 6x6, 8x8, ..., 64x64 pixels. In this paper they are referred to as BOX32 and BOX64 respectively.

In order to define a closed-loop jet boundary for fractal analysis of the jet images in Fig. 1, one needs to manually select a section of the jet image that excludes regions covering the image of injector tip and the part of the image near the lower edge of the frames. This creates two smooth straight lines joining the left and the right boundaries of the jet at the top and the bottom. The effect of adding these two smooth sections on the fractal dimension value is analyzed by several different methods. First, the left and the right boundaries are manually moved close to each other so the length of the upper smooth line is minimized. The minimization is done on the upper section because the jet diverges downward in the images. Second, the upper and lower smooth lines are replaced by pieces of the right and/or left boundaries of the jet. The fractal dimension increased by 2 to 3 % applying such corrections on the jet images for various chamber pressures. For ease of analysis, however, we determine the fractal dimension of jet images with the two upper and lower smooth lines and uniformly apply a 2.5% increase to all final values as a first-degree correction. The selection of the pixel intensity threshold for jet boundary determination is an important factor. For this reason, at each tested chamber pressure the fractal dimensions of the jets are calculated for a wide range of threshold levels and the results are plotted. A maximum excursion of up to 10% is observed at high pressures as the threshold is varied. In most cases, one can detect a plateau region in which a threshold value can be selected. If not, a value at the center of the explored threshold range is chosen. As a cross check, the boundary generated at the chosen threshold is visually overlaid and inspected to follow the original gray scale image as close as is discernable. Figure 2 shows a log-log plot of the number of boxes counted versus the box size for a selected jet at high pressure and for five different threshold levels. On the thresholded images one observes many vein-like structures that are not part of the closed-loop jet boundary but attached to it. These are removed by an appropriately selected sequence of erosion/dilation image processing cycles. Special treatment is also required for images at low pressures (i.e. the subcritical regime). The boundary of the jet is determined such that all isolated and single-pixel touching ligaments and drops are excluded. This is achieved by application of series of erosion and dilation steps as described in *Russ[13]*.

In the past ten years a number of applications of fractal analysis have been demonstrated in different disciplines. For example, *Sreenivasan and Meneveau [18]* computed the box-counting and Minkowski fractal dimension of the turbulent boundary of a smoke-tagged turbulent gas jet visualized across its diameter using a laser sheet, where the laser sheet thickness was smaller or comparable to Kolmogorov scale to minimize "fuzzing" due to the finite thickness of the sheet. *Sreenivasan [19]* summarized the results and reported fractal dimensions of 1.35, 1.34, and 1.38 for a round gaseous jet, a plane gaseous mixing layer, and a boundary layer flow, respectively, using two-dimensional digital imaging from LIF visualizations. At atmospheric pressure, *Shavit and Chigier [20]* established a relationship between the peak of the fractal dimension calculated at different streamwise directions and the breakup point as well as the intact length of a jet (or spray) produced by a coaxial air-assist injector. They report the peak-value dimension to range from 1.12 to 1.32 as the air speed is increased from 30 to 90 m/s. It is also interesting to mention that *Mantzaras et al [21],* who measured the Minkowski dimension of flames in spark-ignited engines, and *North and Santavicca [22]*, who measured the Minkowski dimension of atmospheric pressure premixed flames, both report a progressive increase in the fractal dimension from 1.05 to 1.36 as the turbulence level is increased. This indicates a progressive wrinkling and space-filling of the flame front by turbulence. Finally, modeling turbulent flames using fractal concepts is discussed in *Gouldin [23]* and *Gouldin et al. [24].*

Fractal dimension measurements of the nitrogen jet images are plotted as a function of the reduced pressure (chamber pressure divided by the critical pressure of nitrogen) in Fig. 3. Separate curves are shown for the BOX32, BOX64, and EDM methods, and a fourth curve plots the average of all three. The value of the fractal dimension at each pressure is the average of 18 to 20 images. The BOX64 method produces systematically higher measurements than the other two, which is believed to be due to contributions beyond the 32x32 grid size. Considering the better accuracy of the EDM method and its closeness to the BOX32 results, the latter two methods are considered to produce more representative measurements of the fractal dimension. Also plotted in Fig. 3 are fractal dimensions measured by other researchers of liquid sprays and gaseous jets, mixing layers, and boundary layers. The measurements reported for *Dimotakis et al. [25]* and *Taylor and Hoyt [27]* are our measurements made from scanned images of pictures contained in those references.

The general trend of all the curves in Fig. 3 is that the fractal dimension increases as the chamber pressure increases. At low pressures, the trend of the curves is towards the Euclidian value of 1 for a smooth circular cylinder with no surface irregularities. The magnitude of the measurements at the lowest pressures where the jets are subcritical is consistent with the fractal dimension of a 2nd wind-induced spray measured from the scanned images of *Taylor and Hoyt [27].* As pressure increases, a dip in the curves occurs at a reduced pressure of about 0.9, due to a transition out of the 2nd wind-induced atomization regime. At the highest pressures where the jets are supercritical, the magnitude of the fractal dimension becomes consistent with the fractal dimensions of gaseous jets and layers.

These results support the hypothesis that subcritical jets exhibit mainly spray-like behavior, while supercritical jets exhibit mainly gas-like behavior. Earlier support for this hypothesis included qualitative observations of the jet appearance and the quantitative spreading rate measurements of *Chehroudi, et. al. [8].* The present fractal dimension measurements constitute the second quantitative respect and the third overall respect in which the hypothesis is true.

Summary and Conclusions

The fractal dimensions of round turbulent cryogenic nitrogen jets have for the first time been measured at various pressures ranging from subcritical to supercritical. The jets were injected at an initially subcritical temperature into room temperature gaseous nitrogen. A comparison of the box-counting and EDM methods of measuring the fractal dimension revealed the same trends as a function of pressure in all cases, and close quantitative agreement when the box-counting scale is suitably small. At subcritical pressures, the fractal dimension is consistent with a conventional spray in the 2nd wind-induced atomization regime. The fractal dimension tends to increase as pressure increases, until at supercritical pressures the fractal dimension is consistent with those of gaseous jets and layers. These results constitute further quantitative evidence that subcritical jets exhibit mainly spray-like behavior, and supercritical jets exhibit mainly gas-like behavior.

REFERENCES

1. Mayer, W., Schik, A., Schwitzer, C., and Schaffler, M. "Injection and mixing processes in high pressure LOX/GH2 rocket combustors," AIAA Paper no. 96-2620, Lake Buena Vista, Florida, 1996.
2. Mayer, W., Ivancic, A., Schik, A., and Hornung, U. "Propellant atomization in LOX/GH2 rocket combustors," AIAA Paper no. 98-3685, Cleveland, Ohio, 1998.
3. Chen, L.-D. and Sui, P.-C. "Atomization during the injection of supercritical fluid into high pressure environment," in *Mechanics and Combustion of Droplets in Sprays* by Chiu and Chigier.
4. Woodward , R. D. and Talley, D. G. "Raman imaging of transcritical cryogenic propellants," AIAA Paper 96-0468, Reno, Nevada, January 1996.
5. Harstad, K and Bellan, J. "Isolated fluid oxygen drop behavior in fluid hydrogen at rocket chamber pressures," International Journal of Heat and Mass transfer 41, pp. 3537-3550, 1998.
6. Delplanque J. P. and Sirignano W. A. "Boundary layer stripping effects on droplet transcritical convective vaporization," Atomization and Sprays, 4:325-349, 1994.
7. Oefelein, J. C. and Yang V. "Modeling high-pressure mixing and combustion processes in liquid rocket engines," J. Propulsion & Power, Vol. 14, no. 5, September-October, 1998.
8. Chehroudi, B., Talley, D., and Coy, E. "Visual characteristics and initial growth rates of round cryogenic jets at subcritical and supercritical pressures," Physics of Fluids, Vol. 14, No. 2, February, 2002.
9. Chehroudi, B., Talley, D., and Coy, E. "Fractal geometry and growth rate of cryogenic jets near critical point," AIAA Paper 99-2489, 35th AIAA/ASME/SAE/ASEE Joint Propulsion Conference, Los Angeles, CA, June 20-24, 1999.
10. Chehroudi, B., Cohn, R., Talley, D. and A. Badakhshan. "Raman scattering measurements in the initial region of sub- and supercritical jets," AIAA Paper 99-2489, 36th AIAA/ASME/SAE/ASEE Joint Propulsion Conference, Huntsville, AL, July 17-19, 2000.
11. Mandelbrot, B. B. "The Fractal Geometry of Nature," W. H. Freeman and Company, San Francisco, 1983.
12. Peitgen, H-O, Hartmut, J., Dietmar, S. "Fractals for the Classroom, Part one Introduction to Fractals and Chaos," Springer-Verlag New York Inc., New York, 1992.
13. Russ, J. C. "The image processing handbook: 2nd edition," Boca Raton, FL, CRC Press, Inc. ,P. 674, 1995.
14. Russ, J. C. "Fractal Surfaces," New York: Plenum Press, 1998.

15. Kaye, B H. "Image analysis techniques characterizing fractal structures from the fractal approach to heterogeneous chemistry," (D. Avnir, editor). John Wiley & Sons , 1989.
16. Hall, M. J., Dai, W., and Matthews, R. D. "Fractal analysis of turbulent premixed flame images from SI engines," International Fuel and Lubricants Meeting and Exposition, San Francisco, California, SAE Technical paper 922242, October 19-22, 1992.
17. Russ J. C. and Russ, J. C. "Uses of Euclidean Distance Map for the measurement of features in images," Journal of computer assisted microscopy, Vol.1, no. 4, pp. 343-375, 1989.
18. Sreenivasan, K. R. and Meneveau, C. "The fractal facets of turbulence," J. Fluid Mech. Vol. 173, pp. 357-386, 1986.
19. Sreenivasan, K. R. "Fractals and multifractals in fluid turbulence," Annu. Rev. Fluid Mech, Vol. 23 pp. 539-600, 1991.
20. Shavit, U. and Chigier, N. "Fractal dimensions of liquid jet interface under breakup," Atomization and Sprays, vol. 5, pp. 525-543, 1995.
21. Mantzaras, J., Felton, P. G., and Bracco, F. V. "Fractals and turbulent premixed engine flames," Combustion and Flames, vol. 77, pp. 295-310, 1989.
22. North, G. L. and Santavicca, D. A. "The fractal nature of premixed turbulent flames," Combust. Sci. and Tech., vol. 72, pp. 215-232, 1990.
23. Gouldin, F. C. "An application of fractals to modeling premixed turbulent flames," Combustion and Flames, vol. 68, pp. 249-266, 1987.
24. Gouldin F. C., Hilton, S. M., and Lamb, T. "Experimental evaluation of the fractal geometry of flamelets," Twenty-second Symposium (International) on Combustion/ The combustion Institute, pp. 541-550, 1988.
25. Dimotakis, P. E., Miake-Lye, W. G., and Papantoniou, D. A. "Structure and dynamics of round turbulent jets," Physics of Fluids, 26, no. 11, p. 3185-92.
26. Chehroudi, B., Talley, D., and Coy, E. "Behavior of a round cryogenic jet at below and above the critical pressure." The Tenth Annual Propulsion Symposium, Propulsion Engineering Research Center (PERC) at Penn State, NASA Marshall Space Flight Center, Huntsville, Alabama, October 26-27, 1999.
27. Taylor, J. J. and Hoyt, J. W. "Water jet photography-techniques and methods," Exp. Fluids, Vol. 1, pp. 113-120, 1983.

ACKNOWLEDGEMENT

The authors would like to thank and appreciate the assistance of Mr. Paul Loftsgard in running the fractal analysis program on the jet images.

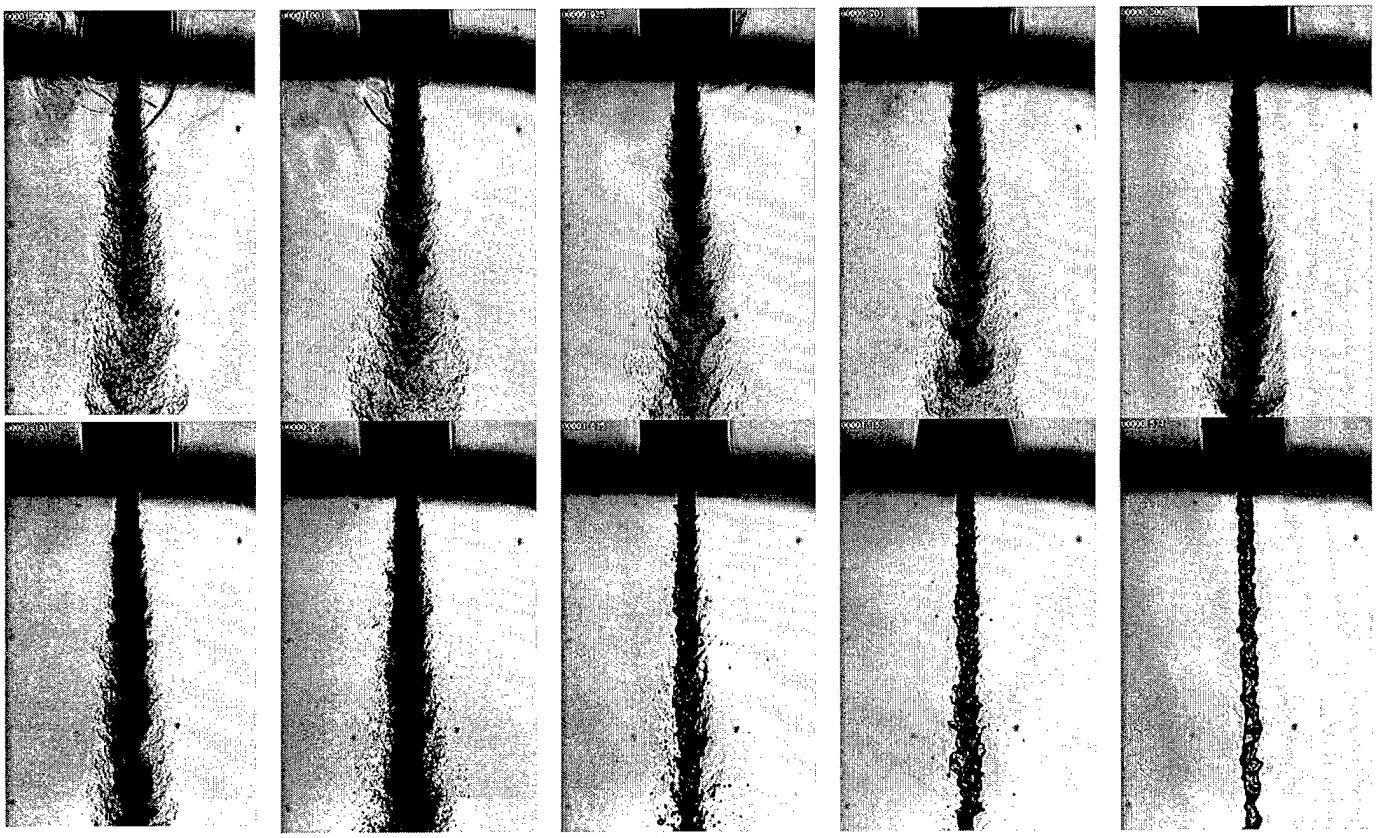

Figure 1. Back-illuminated images of cryogenic nitrogen injected into ambient nitrogen at a fixed supercritical temperature of 300 K but varying sub- to supercritical pressures ($P_{critical}$ = 3.39 MPa; T_c = 126.2 K). Reduced pressure, P_r = $P_{ch}/P_{critical}$= 0.23, 0.43, 0.83, 1.03, 1.22, 1.62, 2.03, 2.44, 2.74; from lower right to upper left. Reynolds number= 25,000 to 75,000. Injection velocity: 10-15 m/s. Froud number: 40,000 to 110,000. Injectant temperature: 99 to 120 K.

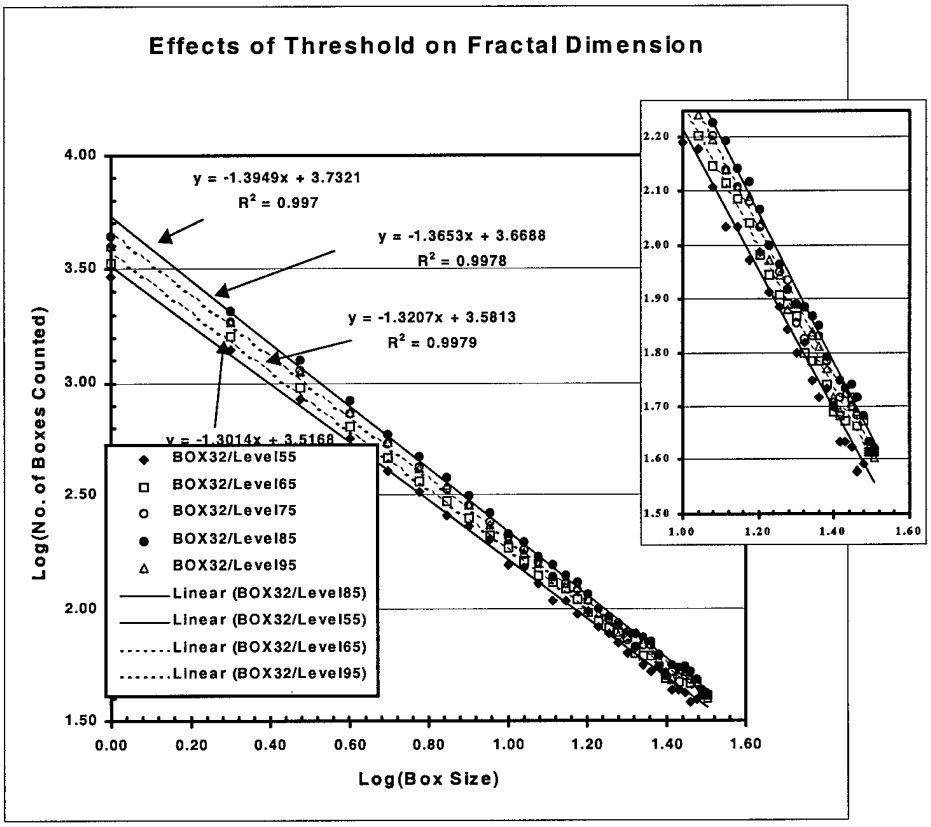

Figure 2. Log-log plot of the number of boxes counted as a function of the box size for four different thresholded binary images of the same original high-chamber-pressure gray-scale jet image indicating effects of the threshold level on the fractal dimension. The slope of the least square fit line is the negative of the box-counting dimension. R^2 is the correlation coefficient of the linear fits.

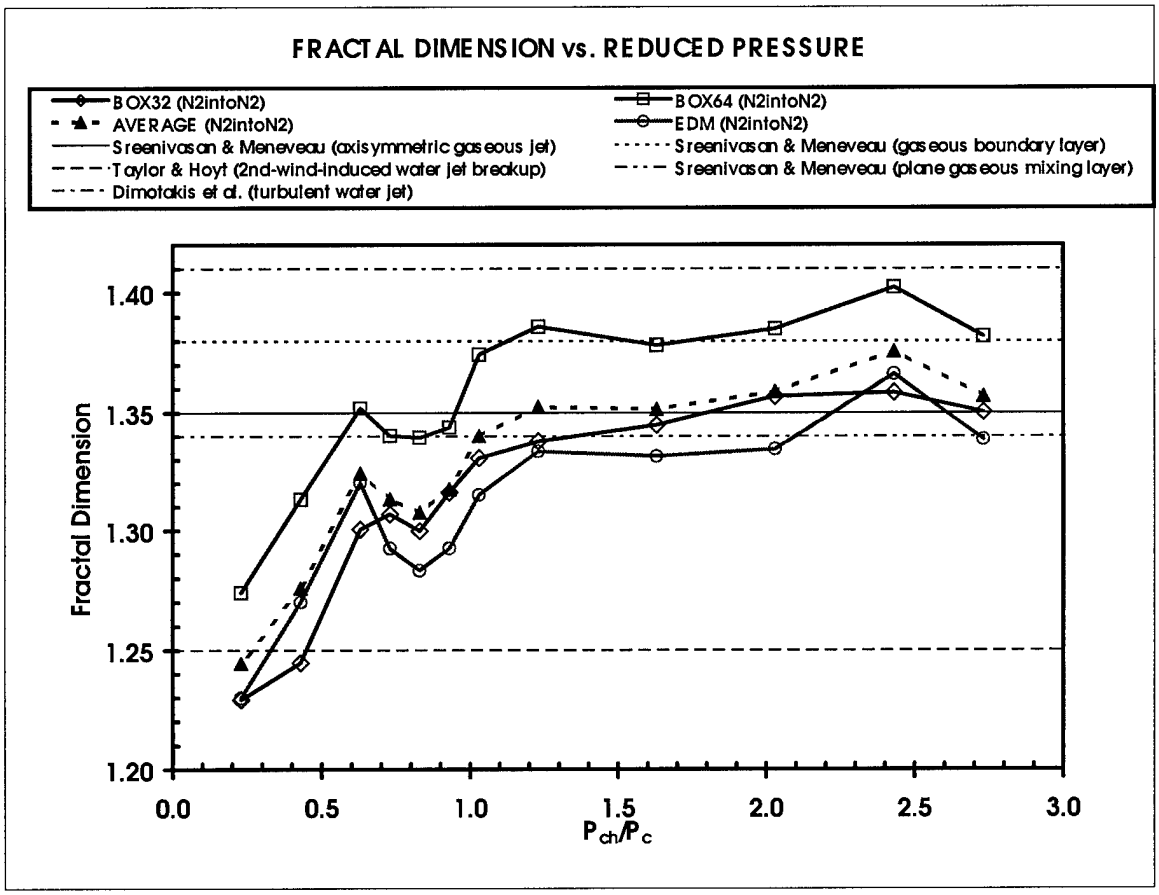

Figure 3. Box-counting and Minkowski (EDM algorithm) fractal dimensions of the visual boundary of the jet as a function of the reduced chamber pressure for N_2-into-N_2 injection. AVERAGE (N2 into N2) is the average of the three shown fractal dimension measurements.